Original Research Article

Numerical Study of Variable Viscosity and Thermal Conductivity on Natural Convection Flow along a Vertical Flat Plate with Pressure Work and Heat Conduction

ABSTRACT

A heated vertical flat plate in the presence of heat generation is an extremely significant technological issue, and many academics have studied this sort of problem. A vertical plate submerged in a fluid with varying viscosity will be used in this research to investigate the effects of variable viscosity and thermal conductivity on heat generation free convection flow. The boundary layer equations in this section are two-dimensional, laminar, and unstable. The fundamental governing equations are turned into non-dimensional governing equations by using the necessary variables. Using the Crank-Nicolson implicit finite-difference technique, these equations are solved numerically. Viscosity and thermal conductivity are temperature-dependent properties of a viscous, incompressible fluid. Variations in the study's numerous parameters will reveal and compare the velocities, temperatures, local skin friction, and local heat transfer co-efficient profiles. There will be a comparison between the current numerical data and previously reported data findings. Besides that, we'll compare our current work numbers to those of past released publications. Graphs and tables will be used to display the findings for a variety of key physical characteristics.

Keywords: Steady State, Heat Generation, Variable Viscosity, Pressure Work, Dependent Thermal Conductivity

1. INTRODUCTION

Natural convection occurs as the fluid's density varies as a result of temperature changes. Because of its widespread usage in both science and engineering, natural convection has piqued the interest of many academics. In addition, scientists and academics are fascinated by the topic of natural convection flow down a vertical flat plate because of the several applications it may potentially serve. This phenomenon is widely seen in the design of microstructures and fluid flows around shrouded heat dissipation fins in a variety of technical applications such as cooling molten metal and nuclear reactors. When it comes to industrial cooling, natural convection is a popular method. The resistance to the flow of fluid is measured by viscosity, which is also a measure of internal fluid friction. To dissipate energy, labor must be done to distort a viscous material. While thermal conductivity, on the other hand, is a measure of heat transport efficiency. Many studies have been conducted on viscous dissipation and thermal conductivity due to their significance.

Effects of variable viscosity and dependent thermal conductivity on free convection flow along a vertical flat plate with heat conduction are significant from the different views. Researcher gets interest in the technology and process for their purpose. Sarker et al. [1] studied the effects of variable viscosity and thermal conductivity on MHD natural convection flow a vertical flat plate. Alam et al. [2] considered the Effect of pressure stress work and viscous dissipation in natural convection flow along a vertical flat plate with heat conduction. Alim et al. [3] investigated the Joule heating effect on the coupling of conduction with MHD free convection flow from a vertical flat plate. Rahman et al. [4] presented the effects of temperature dependent thermal conductivity on MHD free convection flow along a vertical flat plate with heat conduction. Alim et al. [5] studied the combined effect of viscous dissipation & Joule heating on the coupling of conduction & free convection along a vertical flat plate. Molla et al. [6] considered the natural convection laminar flow with temperature

dependent viscosity and thermal conductivity along a vertical wavy surface. Safiqul Islam et al. [7] presented the effects of temperature dependent thermal conductivity on natural convection flow along a vertical flat plate with heat generation. Kabir et al. [8] analyzed the effects of viscous dissipation on MHD natural convection flow along a vertical wavy surface. Viscous and Joule heating effects on MHD free convection flow with variable plate temperature is investigated by Hossain [9]. Finite difference analysis of transient free convection on an isothermal flat plate is studied by Soundalgekar et al. [10]. Steady free convection flow with variable viscosity and thermal diffusivity along a vertical plate is analyzed by Elbashbeshy et al.[11]. The numerical study of the combined free and forced convective laminar boundary layer flow past a vertical isothermal flat plate with temperature dependent viscosity is considered by Kafoussius et al.[13]. The effect of radiation on free convection flow of fluid with variable viscosity from a porous vertical plate is presented by Anwar Hossain et al.[14]. Effect of variable viscosity on a MHD free convection flow past a semi-infinite flat plate with an aligned magnetic field in the case of unsteady flow is studied by Seddeek[15]. G.palani.Kwang et al. [19] studied numerical study on vertical plate with variable viscosity and thermal conductivity. Ullah A et al.[21] considered the Viscoelastic MHD Nanofluid Thin Film Flow over an Unsteady Vertical Stretching Sheet with Entropy Generation. Ullah A Ullah A et al.[22] studied the Non-Linear Thermal Radiations and Mass Transfer Analysis on the Processes of Magnetite Carreau Fluid Flowing Past a Permeable Stretching/Shrinking Surface under Cross Diffusion and Hall Effect. Abdeljawad T et al. [23] has been investigate Thermal Radiations and Mass Transfer Analysis of the Three-Dimensional Magnetite Carreau Fluid Flow Past a Horizontal Surface of Paraboloid of Revolution. *Processes*.

In this work, an analytical solution for the variable viscosity and dependent thermal conductivity in natural convection flow over a vertical flat plate in the presence of heat conduction will be produced based on experimental analysis. The discretization of momentum and energy equations in terms of non-dimensional coordinates X and Y in order to express the equations in finite difference form by approximating functions and derivatives in terms of the central differences in both coordinate directions. The numerical simulations of these equations led to the development of a computer code for the current issue, which uses an efficient implicit finite-difference approach. The Crank-Nicolson scheme is what it's called. For various parameters such as variable viscosity, dependent thermal conductivity, heat generation, pressure work, and Prandtl's number, the outcomes data analysis has developed for velocity profile, temperature profile, local skin friction, local Nusselt number, average skin friction, and average Nusselt number.

2. MATEMATICAL ANALYSIS

The unsteady flow of a viscous incompressible fluid across a semi-infinite vertical plate is considered here. As indicated in Figure1, the $\overline{X}$-axis is taken vertically upward along the plate, and the $\overline{Y}$-axis is picked perpendicular to the plate at the leading edge. The origin of the $\overline{X}$-axis is assumed to lie at the plate's leading edge. Except for the fluid viscosity, which varies exponentially with fluid temperature, the thermal conductivity, which varies linearly with fluid temperature, and the density variation in the body force term in the momentum equation, where the Bossiness approximation is used, all fluid physical properties are assumed to be constant.

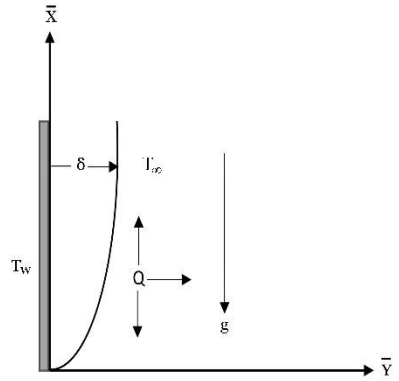

Figure 1: Configuration of vertical flat plate

The mathematical statement of the basic conservation laws of mass, momentum and energy for the steady viscous incompressible and electrically conducting flow, after simplifying we have

$$\frac{\partial \bar{U}}{\partial \bar{X}}+\frac{\partial \bar{V}}{\partial \bar{Y}}=0 \tag{1}$$

$$\frac{\partial \bar{U}}{\partial t'}+\bar{U}\frac{\partial \bar{U}}{\partial \bar{X}}+\bar{V}\frac{\partial \bar{U}}{\partial \bar{Y}}=\frac{1}{\rho}\frac{\partial}{\partial \bar{Y}}\left(\mu\frac{\partial \bar{U}}{\partial \bar{Y}}\right)+g\beta\left(T'-T'_{\infty}\right) \tag{2}$$

$$\frac{\partial T'}{\partial t'}+\bar{U}\frac{\partial T'}{\partial \bar{X}}+\bar{V}\frac{\partial T'}{\partial \bar{Y}}=\frac{1}{\rho C_P}\frac{\partial}{\partial \bar{Y}}\left(k\frac{\partial T'}{\partial \bar{Y}}\right)+\frac{T'\beta\bar{U}}{\rho C_p}\frac{\partial P}{\partial \bar{X}}+\frac{Q_0}{\rho C_P}\left(T'-T'_{\infty}\right) \tag{3}$$

Where, $\bar{U}$ and $\bar{V}$ are the velocity components along the $\bar{X}$ and $\bar{Y}$ axis respectively, t' is the time, T' is the temperature of the fluid in the boundary layer and T'_{∞} is the fluid temperature far away from the plate , g is the acceleration due to gravity, κ is the thermal conductivity of the fluid, ρ is the density, C_p is the specific heat at constant pressure and μ is the variable dynamic co-efficient of viscosity of the fluid. The amount of heat generated or absorbed per unit volume is $Q_0\left(T-T_{\infty}\right)$, Q_0 being a constant, which may take either positive or negative and the hydrostatic pressure $\frac{\partial P}{\partial \bar{X}}=-\rho_e g$ where, $\rho_e=\rho$. The source term represents the heat generation when $Q_0 > 0$ and the heat absorption when $Q_0 < 0$. $k(T)$ is the thermal conductivity of the fluid depending on the fluid temperature T', σ_0 is the electric conduction and β_0 is the magnetic field strength.

The initial and boundary conditions are

$$\begin{aligned}
&t' \le 0:\ \bar{U}=0, \bar{V}=0, \quad T'=T'_{\infty} \text{ for all } Y\\
&t' > 0:\ \bar{U}=0, \bar{V}=0, \quad T'=T'_{w} \text{ at } Y=0\\
&t' > 0:\ \bar{U}=0, T'=T'_{\infty} \text{ at } \bar{X}=0\\
&t' > 0:\ \bar{U}\to 0, \quad T'\to T'_{\infty} \text{ as } \bar{Y}\to\infty
\end{aligned} \tag{4}$$

On introducing the following non-dimensional quantities in equations (2.1) to (2.4), we have

$$X=\frac{\bar{X}}{L},\ Y=\frac{\bar{Y}}{L}Gr^{1/4},\ U=\frac{L\bar{U}}{\nu}Gr^{-1/2},\ V=\frac{\bar{V}L}{\nu}Gr^{-1/4},\ t=\frac{\nu t'}{L^2}Gr^{1/2}, \tag{5}$$

$$T=\frac{T'-T'_{\infty}}{T'_{w}-T'_{\infty}},\ Gr=\frac{g\beta L^3\left(T'_{w}-T'_{\infty}\right)}{\nu^2},\ \Pr=\frac{\mu_0 C_p}{k_0},\ \nu=\frac{\mu_0}{\rho}$$

Here *L* is the length of the plate, ν is the kinematic viscosity, Gr is the Grashof number, Pr is the Prandtl number. Out of many forms of variation of viscosity and thermal conductivity with dimensionless temperature T, which are available in the literature. The following forms are proposed by Stattery[21], Ockendon and Ockendon[8], Elbashbeshy and Ibrahi[10], Wilson and Duffy[16], and Seddeek and Abdelmegguid[19]

$$\frac{\mu}{\mu_0}=e^{-\lambda T} \tag{6}$$

$$\frac{k}{k_0}=1+\gamma T \tag{7}$$

Where λ and γ denote the viscosity and thermal conductivity variation parameters respectively, depended on the nature of the fluid. Here μ_0 and k_0 are the viscosity and the thermal conductivity at temperature T'_w.

The magneto hydrodynamic field in the fluid is governed by the boundary layer equations, which in the non-dimensional form obtained by introducing the dimensionless variables described in (5), may be written the equation of continuity as

$$\frac{\partial \bar{U}}{\partial \bar{X}}+\frac{\partial \bar{V}}{\partial \bar{Y}}=0$$

$$\Rightarrow \frac{\partial(\frac{\upsilon}{L}Gr^{\frac{1}{2}}U)}{\partial(X\,L)}+\frac{\partial(\frac{\upsilon}{L}Gr^{\frac{1}{4}}V)}{\partial(\frac{Y\,L}{Gr^{-\frac{1}{4}}})}=0$$

$$\Rightarrow \frac{\frac{\upsilon}{L}Gr^{\frac{1}{2}}}{L}\frac{\partial U}{\partial X}+\frac{\frac{\upsilon}{L}Gr^{\frac{1}{4}}}{\frac{L}{Gr^{\frac{1}{4}}}}\frac{\partial V}{\partial Y}=0$$

$$\therefore \frac{\partial U}{\partial X}+\frac{\partial V}{\partial Y}=0 \qquad (8)$$

Now momentum equation (2) can be reduced by applying the non- dimensional transformation (5) and (6), we have

$$\frac{\partial \bar{U}}{\partial t'}+\bar{U}\frac{\partial \bar{U}}{\partial \bar{X}}+\bar{V}\frac{\partial \bar{U}}{\partial \bar{Y}}=\frac{1}{\rho}\frac{\partial}{\partial \bar{Y}}\left(\mu\frac{\partial \bar{U}}{\partial \bar{Y}}\right)+g\beta\left(T'-T'_{\infty}\right)$$

$$\Rightarrow \frac{Gr\nu^2}{L^3}\frac{\partial U}{\partial t}+\frac{Gr\nu^2}{L^3}u\frac{\partial U}{\partial X}+\frac{Gr\nu^2}{L^3}V\frac{\partial U}{\partial Y}$$

$$=\frac{1}{\rho}\frac{\nu Gr\mu_0}{L^3}\frac{\partial}{\partial Y}\left(e^{-\lambda T}\frac{\partial U}{\partial Y}\right)+g\beta(T'_w-T'_{\infty})$$

$$\Rightarrow \frac{\partial U}{\partial t}+u\frac{\partial U}{\partial X}+V\frac{\partial U}{\partial Y}=\left[e^{-\lambda T}\frac{\partial^2 U}{\partial Y^2}-\lambda e^{-\lambda T}\frac{\partial T}{\partial Y}\frac{\partial U}{\partial Y}\right]+T$$

$$\Rightarrow \frac{\partial U}{\partial t}+u\frac{\partial U}{\partial X}+V\frac{\partial U}{\partial Y}=\left[e^{-\lambda T}\frac{\partial^2 U}{\partial Y^2}-\lambda e^{-\lambda T}\frac{\partial T}{\partial Y}\frac{\partial U}{\partial Y}\right]+T \qquad (9)$$

Again, the energy equation (3) can be reduced by the above similarity transformation (5) and (7), we have

$$\frac{\partial T'}{\partial t'}+\bar{U}\frac{\partial T'}{\partial \bar{X}}+\bar{V}\frac{\partial T'}{\partial \bar{Y}}=\frac{1}{\rho C_P}\frac{\partial}{\partial \bar{Y}}\left(k\frac{\partial T'}{\partial \bar{Y}}\right)+\frac{T'\beta\bar{U}}{\rho C_p}\frac{\partial P}{\partial \bar{X}}+\frac{Q_0}{\rho C_P}\left(T'-T'_{\infty}\right)$$

$$\Rightarrow \frac{\partial T}{\partial t}+U\frac{\partial T}{\partial X}+V\frac{\partial T}{\partial Y}=\frac{k_0}{\mu_0 C_P}\left\{(1+\gamma T)\frac{\partial^2 T}{\partial Y^2}+\gamma\left(\frac{\partial T}{\partial Y}\right)^2\right\}$$

$$+\frac{\left\{\frac{T'_{\infty}+T\left(T'_w-T'_{\infty}\right)}{T'_w-T'}\right\}L\beta u}{\rho C_p}\left(-\rho_e g\right)+\frac{Q_0L^2}{\rho C_P\nu Gr^{1/2}}\frac{\left(T'-T'_{\infty}\right)}{\left(T'_w-T'\right)}$$

$$\Rightarrow \frac{\partial T}{\partial t}+U\frac{\partial T}{\partial X}+V\frac{\partial T}{\partial Y}=\frac{1}{P_r}\left[\gamma\left(\frac{\partial T}{\partial Y}\right)^2\right]+\frac{1}{P_r}\left[\left(1+\gamma T\right)\frac{\partial^2 T}{\partial Y^2}\right] \tag{10}$$

$$-\left\{\left(T+\frac{T'_\infty}{\left(T'_w-T'_\infty\right)}\right)\right\}G_e u+QT$$

The Corresponding initial condition and boundary condition in a dimensionless forms are as follows

$$t\le 0:\ U=0, V=0,\quad T=0\sqrt{b^2-4ac}\ \text{ for all } Y$$

$$t\rangle 0:\ U=0, V=0,\quad T=1\ \text{ at } Y=0$$

$$U=0,\quad T=0\ \text{ at } X=0 \tag{11}$$

$$U\to 0,\quad T\to 0\quad at\ Y\to\infty$$

Equations (8) to (11) with the boundary condition (11) describe the free convective unsteady laminar boundary layer flow with variable viscosity and thermal conductivity along an isothermal semi-infinite vertical plate.

Where, $\Pr=\mu_0 C_p/k_0$, the Prandtl's number, $Q_0L^2/\mu C_P Gr^{1/2}=Q$ is the heat generation parameter and $Ge=g\beta L/C_p$ is the pressure work parameter.

The local shear stress in the plate is defined by

$$\tau_{\bar{X}}=\left(\mu\frac{\partial\bar{U}}{\partial\bar{Y}}\right)_{\bar{Y}=0} \tag{12}$$

By introducing the non-dimensional quantities given in equations (5)-(6) in (12), we get non-dimensional form of local skin friction and it is given by

$$\tau_{\bar{X}}=\left(\mu\frac{\partial\bar{U}}{\partial\bar{Y}}\right)_{\bar{Y}=0}$$

$$\Rightarrow \frac{L^2}{\nu\mu_0}\tau_{(X\,L)}=Gr^{\frac{3}{4}}e^{-\lambda}\left[\frac{\partial U}{\partial Y}\right]_{Y=0}$$

$$\therefore \bar{\tau}_X=Gr^{\frac{3}{4}}e^{-\lambda}\left[\frac{\partial U}{\partial Y}\right]_{Y=0} \tag{13}$$

The integration of equation (2.13) from $X=0$ to $X=1$ gives the average skin friction and it is given by

$$\bar{\tau}=e^{-\lambda}Gr^{\frac{3}{4}}\int_0^1\left(\frac{\partial U}{\partial Y}\right)_{Y=0}d\,X\sqrt{a^2+b^2} \tag{14}$$

The local Nusselt number is defined by

$$Nu_{\bar{X}} = \frac{-L\left(k\frac{\partial T'}{\partial \bar{Y}}\right)_{\bar{Y}=0}}{k_0\left(T'_w - T'_\infty\right)}$$

$$\Rightarrow Nu_{(X\,L)} = -L\left[\frac{k_0\left(1+\gamma T\right)}{k_0\left(T'_w - T'_\infty\right)LGr^{-\frac{1}{4}}}\left(\frac{\partial T}{\partial Y}\right)_{Y=0}\right]$$

$$\Rightarrow Gr^{-\frac{1}{4}}\left(T'_w - T'_\infty\right)Nu_{(X\,L)} = -\left(1+\gamma\right)\left(\frac{\partial T}{\partial Y}\right)_{Y=0} \quad \because Y=0, T=1$$

$$\Rightarrow \bar{N}u_X = -\left(1+\gamma\right)\left(\frac{\partial T}{\partial Y}\right)_{Y=0}$$

$$\therefore \bar{N}u_X = -\left(1+\gamma\right)\left(\frac{\partial T}{\partial Y}\right)_{Y=0} \tag{15}$$

The integration of equation (15) from $X=0$ to $X=1$ gives the average skin friction and it is given by

$$\therefore Nu_X = -\left(1+\gamma\right)\int_0^1\left(\frac{\partial T}{\partial Y}\right)_{Y=0} dX \tag{16}$$

2.1 Numerical Techniques

The two-dimensional, non-linear, unsteady and coupled partial differential Equations (8)-(10) under the initial and boundary conditions in Equation (11) are solved using an implicit finite difference scheme of Crank-Nicol-son type which is fast convergent and unconditionally stable. The finite difference equation corresponding to Equations (8) to (10) are given by

$$\frac{\left[U_{i,j}^{k+1} - U_{i-1,j}^{k+1} + U_{i,j}^{k} - U_{i-1,j}^{k} + U_{i,j-1}^{k+1} - U_{i-1,j-1}^{k+1} + U_{i,j-1}^{k} - U_{i-1,j-1}^{k}\right]}{4\Delta X} + \frac{\left[V_{i,j}^{k+1} - V_{i,j-1}^{k+1} + V_{i,j}^{k} - V_{i,j-1}^{k}\right]}{2\Delta Y} = 0 \tag{17}$$

$$\frac{\left[U_{i,j}^{k+1} - U_{i,j}^{k+1}\right]}{2\Delta t} + U_{i,j}^{k}\frac{\left[U_{i,j}^{k+1} - U_{i-1,j}^{k+1} + U_{i,j}^{k} - U_{i-1,j}^{k}\right]}{2\Delta X}$$

$$V_{i,j}^{k}\frac{\left[U_{i,j+1}^{k+1} - U_{i,j-1}^{k+1} + U_{i,j+1}^{k} - U_{i,j-1}^{k}\right]}{4\Delta Y} = \frac{1}{2}\left[T_{i,j}^{k+1} + T_{i,j}^{k}\right]$$

$$++e^{-\lambda}\left[\frac{T_{i,j}^{k+1} + T_{i,j}^{k}}{2}\right]\frac{\left[U_{i,j-1}^{k+1} - 2U_{i,j}^{k+1} + U_{i,j+1}^{k} + U_{i,j-1}^{k} - 2U_{i,j}^{k} + U_{i,j+1}^{k}\right]}{2(\Delta Y)^2}$$

$$-\lambda e^{-\lambda}\left[\frac{T_{i,j}^{k+1} + T_{i,j}^{k}}{2}\right]\frac{\left[T_{i,j+1}^{k+1} - T_{i,j-1}^{k+1} + T_{i,j+1}^{k} - T_{i,j-1}^{k}\right]}{4\Delta Y}\frac{\left[U_{i,j+1}^{k+1} - U_{i,j-1}^{k+1} + U_{i,j+1}^{k} - U_{i,j-1}^{k}\right]}{4\Delta Y} \tag{18}$$

$$\left[\frac{T_{i,j}^{k+1} - {}_{i,j}^{k}}{2\Delta t}\right] + U_{i,j}^{k}\frac{\left[T_{i,j}^{k+1} - T_{i-1,j}^{k+1} + T_{i,j}^{k} - T_{i-1,j}^{k}\right]}{2\Delta X} + V_{i,j}^{k}\frac{\left[T_{i,j-1}^{k+1} - T_{i,j-1}^{k+1} + T_{i,j+1}^{k} - T_{i,j-1}^{k}\right]}{4\Delta y}$$

$$= \frac{1+\gamma T_{i,j}^{k}}{\mathrm{Pr}}\frac{\left[T_{i,j-1}^{k+1} - 2T_{i,j}^{k+1} + T_{i,j+1}^{k} + T_{i,j-1}^{k} - 2T_{i,j}^{k} + T_{i,j+1}^{k}\right]}{2(\Delta Y)^2}$$

$$+\frac{\gamma}{\Pr}\left[\frac{\left[T_{i,j+1}^{k+1}-T_{i,j-1}^{k+1}+T_{i,j+1}^{k}-T_{i,j-1}^{k}\right]}{4\Delta Y}\right]-\left[\frac{1}{2}\left\{T_{i,j}^{k+1}+T_{i,j}^{k}\right\}+\frac{T'_{\infty}}{T'_{w}-T'_{\infty}}\right]\frac{1}{2}\left(U_{i,j}^{k+1}+U_{i,j}^{k}\right)Ge$$
$$+\frac{Q}{2}\left[T_{i,j}^{k+1}+T_{i,j}^{k}\right] \quad (19)$$

The region of integration is considered as a rectangle with sides X_{max}(= 1) and Y_{max}(= 10), where Y_{max} Corresponds to $Y=\infty$, which lies very well outside the momentum and energy boundary layers. The maximum of *Y* was chosen as 6 after some preliminary investigations so that the last two of the boundary conditions (11) are satisfied. Here, the subscript *i*-designates the grid point along the *U*-direction, *j*-along the *V*-direction and the superscript *k* along the *t*-direction. During any one-time step, the coefficients $U_{i,j}^{k}$ and $V_{i,j}^{k}$ appearing in the difference equations are treated as constants. The values of *U, V* and *T* are known at all grid points at *t* = 0, from the initial conditions. The computations of *U, V* and *T* at time level *(k* + 1) using the values at previous time level (fe) are carried out as follows: the finite difference Eq. (18) at every internal nodal point on a particular *i*-level constitute a tridiagonal system of equations. Such a system of equations is solved by Thomas algorithm as described in Carnahan *et al*. [19]. Thus, the values of *T* are found at every nodal point for a particular *i* at *(k* + l)th time level. Using the values of *T* at *(k* + *1)*th time level in the Eq. (13), the values of *u* at *(k* + 1)th time level are found in a similar manner. Thus, the values of *T* and *U* are known on a particular *i*-level. Finally, the values of *V* are calculated explicitly using the Eq. (12) at every nodal point on a particular *i*-level at *(k* + 1)th time level. This process is repeated for various *i*-levels. Thus the values of *T, U* and *V* are known, at all grid points in the rectangular region at *(k* + 1)th time level.

After considering with few sets of mesh sizes, they have been fixed at the level ΔX = 0.05, ΔY = 0.25, and the time step Δt = 0.01. In this case, spatial mesh size is reduced by 50% in one-direction then in both directions, and the results are compared. It is observed that, when mesh size is reduced by 50% in *X*-direction and *Y*-direction the results differ in fourth decimal place. Hence the above-mentioned sizes have been considered as appropriate mesh size for calculations. Computations are carried out until the steady-state is reached. The steady-state solution is assumed to have been reached, when the absolute difference between the values of *U,* as well as temperature *T* at two consecutive time steps are less than 10^{-5} at all grid points. The local truncation error is *O* ($\Delta f^2 + \Delta F^2 + \Delta AX$) and it tends to zero as Δt. ΔX and ΔY tend to zero, which shows that the scheme is compatible. Also, the Crank-Nicolson type of implicit finite difference scheme is proved to be unconditionally stable for a natural convective flow in which there is always a non-negative value of velocity *U* and a non-positive value of V. Thus, compatibility and stability ensure the implicit finite difference scheme is convergent.

3. RESULTS AND DISCUSSION

The direct microscopic exchange of kinetic energy of particles via the border between two systems is known as heat conduction, sometimes known as diffusion. Water is an excellent heat transfer fluid because of its large thermal capacity and low viscosity. Oil has a greater liquid temperature than water, therefore it's been a popular alternative for avoiding the problem of high pressure. Heat is transferred between the Earth's surface and the atmosphere by conduction, radiation, and convection. Heat is transferred via convection when a heated fluid, such as air or water, is forced to flow away from the source of heat, carrying energy with it. Convection happens when hot air expands, becomes less dense, and rises above a heated surface. Because liquid metals have a low Prandtl's number, heat transmission through molecular thermal conduction is important not only in the near-wall layer, but also in the flow core, even in a fully developed turbulent flow.

The following ranges forλ, γ and *Pr* are considered in the present study are:

For air: $-0.7 \le \lambda \le 0$, $0 \le \gamma \le 6$, $Pr = 0.733$

For water: $0 \le \lambda \le 0.6$, $0 \le \gamma \le 0.12$, $2 \le Pr \le 7.00$

In order to check the accuracy of our computed values, we compare our results with the curves computed by G.palani.Kwang-Yong Kim and Elbashbeshy & Ibrahim for various values of λ and γ for air *(Pr* = 0.733). These are plotted in Figs. 2(a), 2(b). Our results agree very well with those of G.palani.Kwang-Yong Kim and Elbashbeshy & Ibrahim at the steady state.

During the initial period the following step changes in the wall temperature, the body force have not had sufficient time to generate and appropriate motion in the fluid. Hence the velocity components *U* and *V* both are negligible for small time *t.* During this initial transient regime, the heat transfer are dominated by pure heat conduction, and hence for constant viscosity and thermal conductivity. Equation (10) reduces to

$$\frac{\partial T}{\partial t} = \frac{1}{\Pr}\frac{\partial^2 T}{\partial Y^2}$$

Thus, for short times, it is noted that for a given Prandtl's number, magnetic parameter, the temperature profile is a function of time only and normal distance from the wall. Setting *Pr* = 1, the solutions of Eq. (15) subject to the initial and boundary conditions given in local Nusellt number are

$$T = erfc\left(\frac{Y}{2\sqrt{t}}\right) \tag{20}$$

Figures 3(a), 3(b), 4(a), 4(b), 5(a), 5(b), 6(a) 6(b), 7(a), 7(b), 8(a), 8(b), 9(a), 9(b), 10(a), 10(b), 11(a), 11(b) shows that the variation of velocity and temperature at their transient, temporal maximum and steady state against the co-ordinate *Y* at the leading edge of the plate viz., *X* = 1.0 for variable viscosity, thermal conductivity, heat conduction variation parameters, pressure work parameters and Prandtl's numbers. The fluid velocity increases and reached its maximum value at very near to the wall (i.e., $0 \le Y \le 2$) and then decreases monotonically to zero as *Y* becomes large for all time *t.* It is also observed that the velocity and temperature increases with time *t*, reaches a temporal maximum and consequently it reaches the steady state.

Figures 3(a) and 3(b) shows that the variation of transient velocity and temperature profiles with area *A*. for a fixed value of γ = 1.00 in air (*Pr* = 0.733), Ge=0.20 and *Q* = 0.50. The velocity of the fluid increases with time until a temporal maximum is reached and thereafter a moderate reduction is observed until the ultimate steady state is reached. It is observed that the time taken to reach the steady state decreases marginally with an increasing the viscosity variation parameter. From Fig. 3(a), it is clear that velocity *U* at any vertical plane near to the plate increases as *X* increases (the viscosity of air decreases). But an opposite trend is observed at a certain distance from the wall. From Fig. 3(b), it is observed that the temperature of the fluid decreases as λ increases (the viscosity of air decreases).

The numerical values of the variation of transient velocity and temperature profiles with γ for a fixed value of λ = - 0.30, *Q* = 0.40, Ge=0.10 in air (*Pr* = 0.733) with the variation of thermal conductivity parameter γ are shown graphically in Figs. 4(a) and 4(b). From these figures, it is observed that the velocity and temperature distribution in the fluid increases as γ increases (thermal conductivity of air increases) for fixed value of λ, *Q* and Prandtl's number. It can also be noticed that with an increase in γ, the rise in the magnitude of the velocity and temperature is significant, which implies that the volume flow rate increases with an increase in γ. The effect of variation of thermal conductivity on velocity and temperature is more significant even in the initial transient period. Also, it is observed that the time to reach the temporal maximum and steady state decreases with increasing thermal conductivity parameter,γ.

The numerical values of variation velocity and temperatures are calculated from Eqs. (13) and (14) are depicted in the graphical form in the Figs. 5(a) and 5(b) for various values of λ for fixed value of *Q* = 0.60,Ge=0.30, γ = - 0.40 in water (*Pr* = 3.00). It is clearly noticed that the time taken to reach the temporal maximum and steady state decreases with an increasing the viscosity variation parameter, λ. It can be seen from Fig. 5(a) that an increase in the viscosity variation parameter, λ increases the velocity of the flow near the wall, because the viscosity of water decreases with an increase of the viscosity variation parameter, λ as seen in Eq.(6). Also, the maximum velocity gets very closer to the wall for higher values of λ. This qualitative effect arises because, for the case of variable viscosity ($\lambda > 0$), the fluid is able to move more easily in a region close to the heated surface in association with the fact that the viscosity of the fluid with $\lambda > 0$ is lower relative to the fluid with constant viscosity. This results in thinner velocity and thermal boundary layers.

It is observed that as λ increases (the viscosity of water decreases), the velocity of the fluid particle increases only in the region $0 \le y \le 2$. From Fig. 5(b), it is noticed that the temperature profiles decrease with increasing λ. This is in association with the fact that an increase in λ yields an increase in the peak velocity. The first effect increases the velocity of the fluid particle, due to the decrease in the viscosity and the second effect decreases the velocity of the fluid particle, due to the decrease in the temperature near the plate, the temperature *T* is high, consequently the first force will be dominant and the velocity *U* increases as λ increases. On the other hand, the temperature *T* is low for far away from the plate, the second effect will be dominant and the velocity decreases as λ increases. From the discussion, we notice that by neglecting the variation of fluid viscosity and thermal conductivity will introduce a substantial error.

Figures 6(a) and 6(b) shows that the variation of velocity and temperature for various values of γ for fixed value of λ = 0.30, *Q* = 0.40, Ge=0.40 in water *(Pr* = 3.00). It is observed that the time taken to reach the steady state decreases with the increasing value of γ. Also, it is observed that the temperature distribution of the fluid increases with the increasing value of γ.

The variation of transient velocity and temperature with Prandtl's numbers for fixed values Pr=3.00, λ = 0.30, Q=0.40 and γ = 0.12 are shown in Figs. 7(a) and 7(b). It is observed that the time taken to reach the temporal maximum and steady state increases with the increasing value of pressure work parameter Ge of the fluid. From the numerical results, we observe that the velocity profile increases with the increasing value of pressure work parameter Ge.

The numerical values of variation of velocity and temperature profiles with *Q*, for a fixed values of λ = 0.50, γ = - 0.10, Ge=0.50 for water (*Pr* = 7.00) are shown graphically in Figs. 8(a) and 8(b). From these figures, it is observed that time taken to reach the steady state is more when the heat generation parameter *Q* increases. Additionally, it is noticed that the velocity Increase as *Q* increases near to the vertical plate. The temperature of the fluid increases as the heat generation parameter *Q* increases.

The variation of transient velocity and temperature with Prandtl's numbers for fixed values Pr=0.733, λ = 0.40, Q=0.40 and γ = 0.30 are shown in Figs. 9(a) and 9(b). It is observed that the time taken to reach the temporal maximum and steady state increases with the increasing value of pressure work parameter Ge of the fluid. From the numerical results, we observe that the velocity profile increases with the increasing value of pressure work parameter Ge.

The variation of transient velocity and temperature with Prandtl's numbers for fixed values of λ = -0.30, γ = 0.40, Ge=0.50 and Q = 0.20 are shown in Figs. 10(a) and 10(b). It is observed that the time taken to reach the temporal maximum and steady state increases with the increasing value of Prandtl's number of the fluid. From the numerical results, we observe that the velocity profile decreases with the increasing value of Prandtl's number. Larger Prandtl's number values give rise to thinner temperature profiles, because a larger Prandtl's number value means that the thermal diffusion from the wall is not prevailing, whereas the velocity diffusion extends far from the wall.

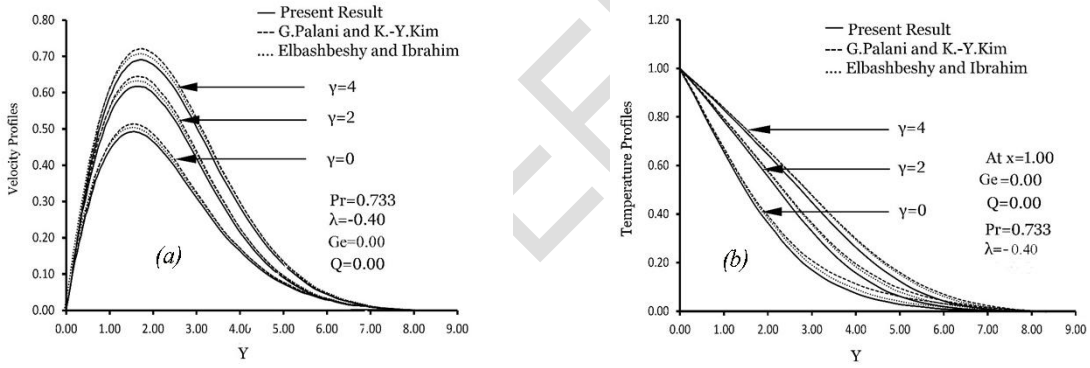

Figures: 2(a) and 2(b), Variation of dimensionless velocity profiles and temperature profiles against dimensionless *Y* for different values of variable thermal conductivity parameter γ with *Pr* = 0.733, λ= 0.40, Ge=0.00 and *Q* = 0.00.

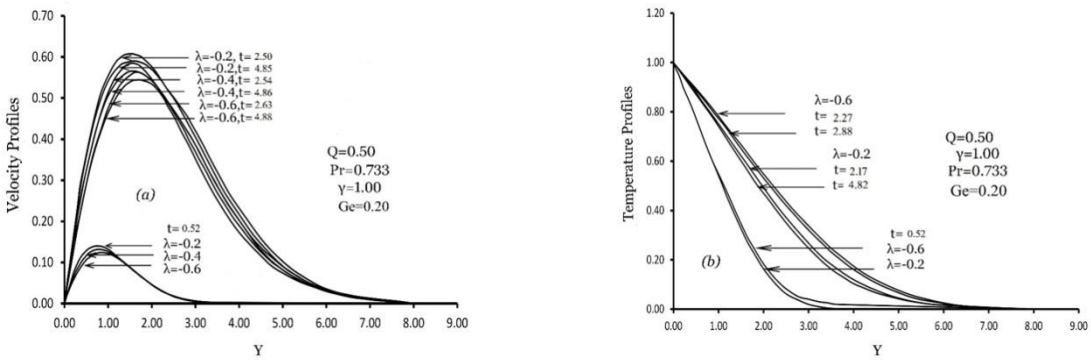

Figures: 3(a) and 3(b), Variation of dimensionless velocity profiles and temperature profiles against dimensionless *Y* for different values of variable viscosity parameter λ and steady state condition with Pr = 0.733, γ = 1.00, Ge=0.20 and *Q*= 0.50.

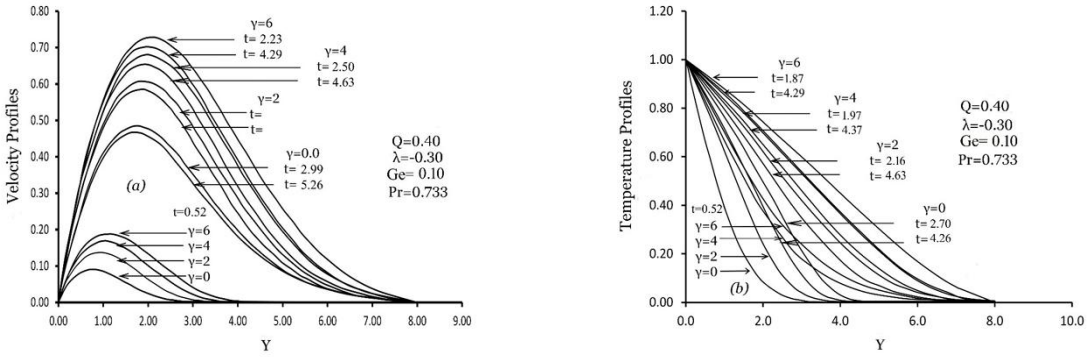

Figures: 4(a) and 4(b), Variation of dimensionless velocity profiles and temperature profiles against dimensionless *Y* for different values of variable thermal conductivity parameter γ and steady state condition with Pr = 0.733, λ = 0.30, Ge=0.10 and *Q* = 0.40.

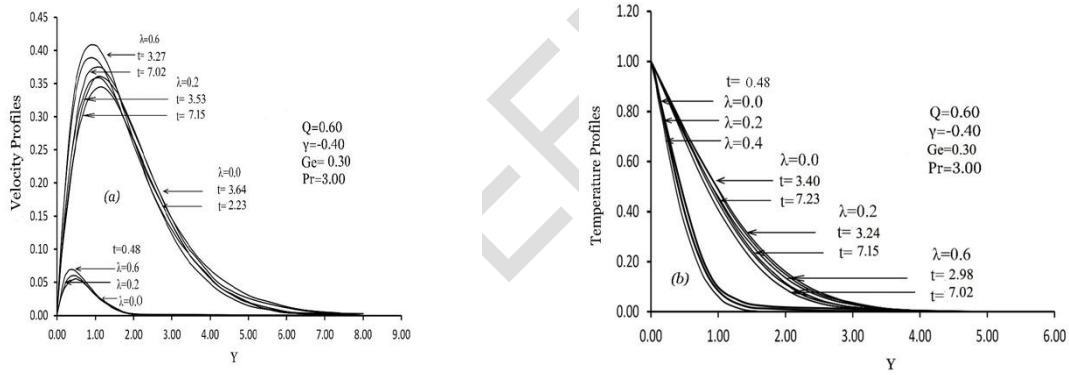

Figures: 5(a) and 5(b), Variation of dimensionless velocity profiles and temperature profiles against dimensionless *Y* for different values of variable viscosity parameter λ and steady state condition with *Pr* = 3.00, γ = 0.40, Ge=0.30 and *Q* = 0.60.

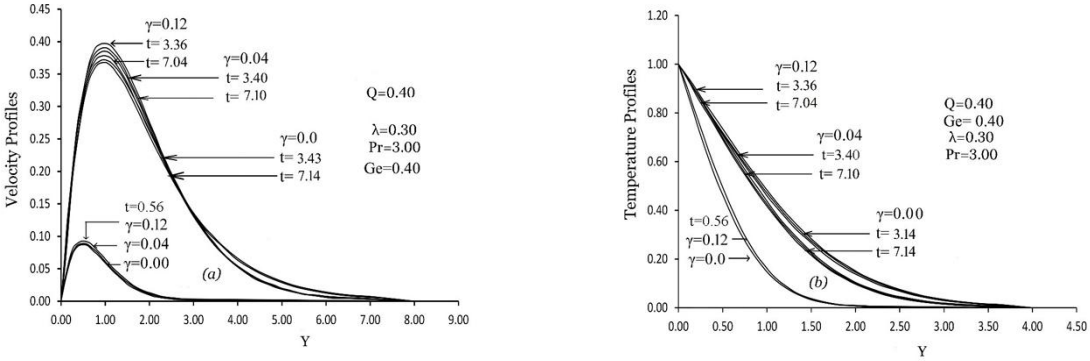

Figures: 6(a) and 6(b), Variation of dimensionless velocity profiles and temperature profiles against dimensionless *Y* for different values of variable thermal conductivity parameter γ and steady state condition with *Pr* =3.00, λ = 0.30, Ge=0.40 and *Q* = 0.40.

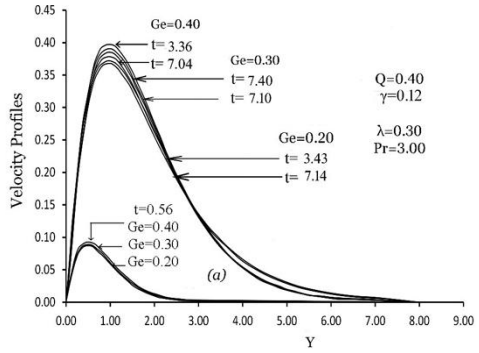

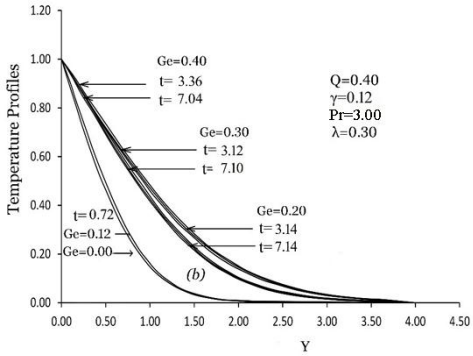

Figures: 7(a) and 7(b), Variation of dimensionless velocity profiles and temperature profiles against dimensionless *Y* for different values of pressure work parameter Ge and steady state condition with λ = 0.30, γ = 0.12, Pr=3.00 and Q = 0.40.

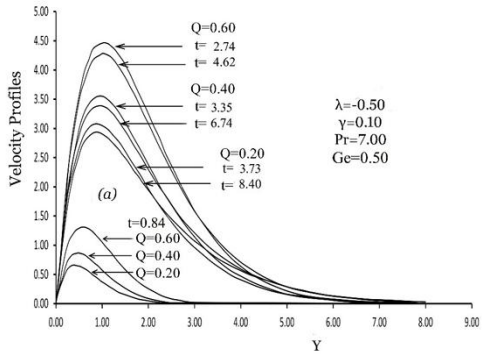

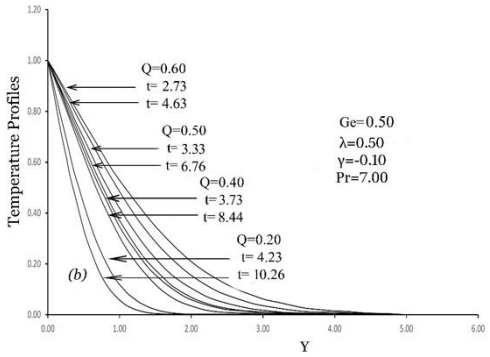

Figures: 8(a) and 8(b), Variation of dimensionless velocity profiles and temperature profiles against dimensionless *Y* for different values of Heat generation parameter *Q* and steady state condition with λ = 0.50, γ = 0.10, Ge=0.50 and *Pr* = 7.00.

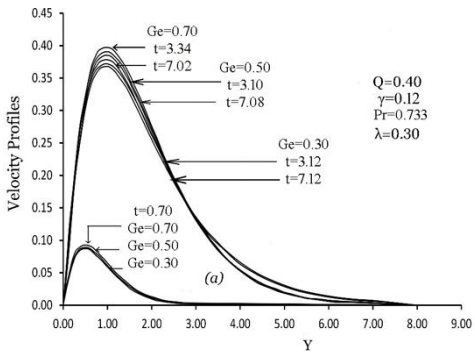

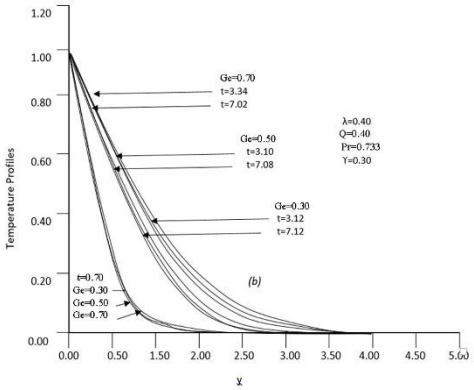

Figures: 9(a) and 9(b), Variation of dimensionless velocity profiles and temperature profiles against

dimensionless *Y* for different values of Pressure Work parameter *Ge* and steady state condition with $\lambda = 0.40$, $\gamma = 0.30$, Q=0.40 and *Pr* = 0.733

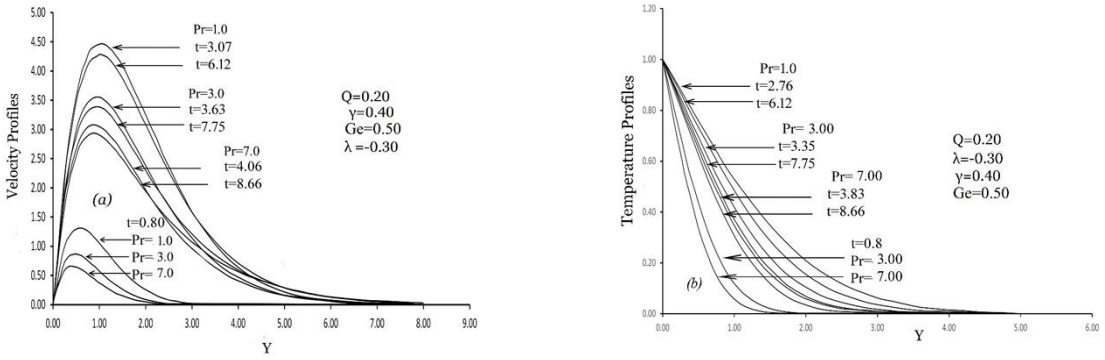

Figures: 10(a) and 10(b), Variation of dimensionless velocity profiles and temperature profiles against dimensionless *Y* for different values of Prandlt's Number *Pr* and steady state condition with $\lambda = 0.30$, $\gamma = 0.40$, Q=0.30 and *Ge* = 0.50

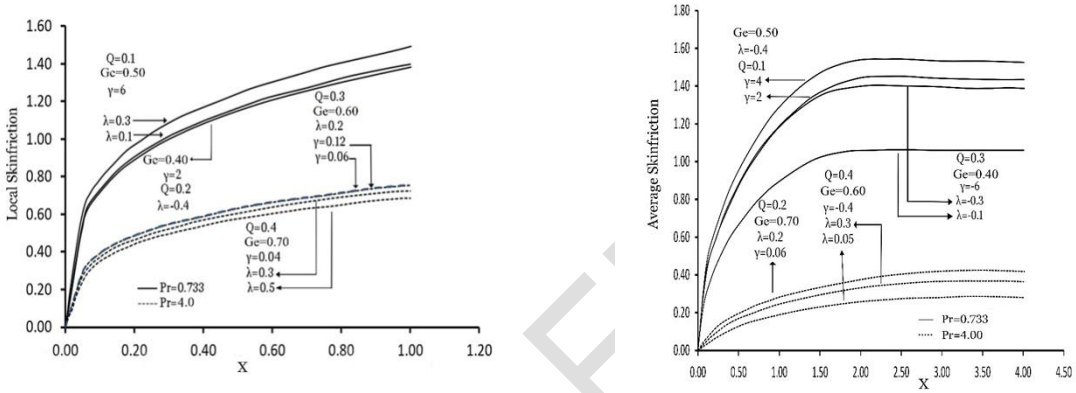

Figures: 11(a) and 11(b), Variation of dimensionless local skin friction and local Nusselt number against dimensionless distance X for different values of *Q, Ge,* λ, γ and *Pr* at steady state condition.

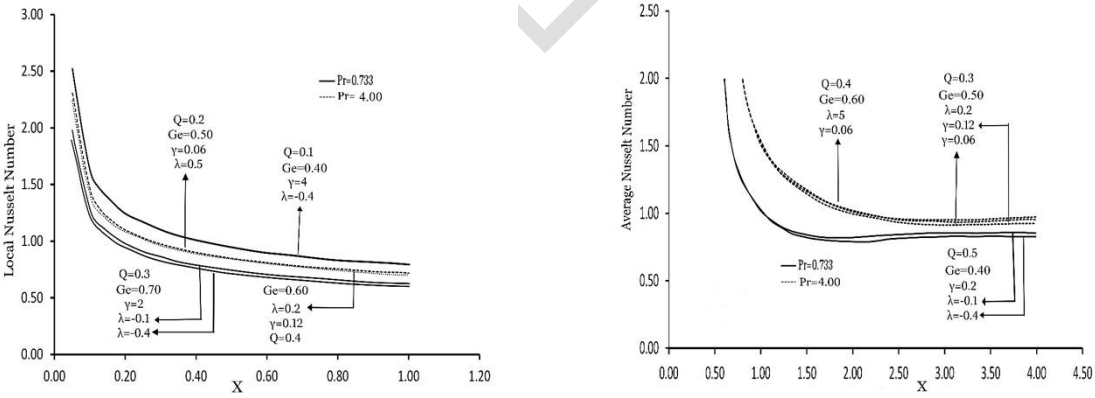

Figures: 12(a) and 12(b), Variation of dimensionless average skin friction and average Nusselt number against dimensionless distance X for different values of *Q, Ge,* λ, γ and *Pr* at steady state condition.

The derivatives involved in Eqs. (12), (14), (15) and (16) are evaluated by using a five point approximation formula and then the integrals are evaluated by Newton-Cotes closed integration formula.

The local skin-friction values are evaluated from Eq. (13) and plotted in Fig. 11(a) as a function of the axial coordinate λ for air and water and selected values of the variation parameters λ and γ. The local skin-friction increases as λ increases. It is observed that local skin friction decreases with the increasing value of viscous variation parameter, λ. It is also

observed that local wall shear stress increases with the increasing value of thermal conductivity parameter, γ. An increase in the value of Prandtl's number, local skin friction is found to decrease.

Average values of skin friction are calculated numerically from the Eq. (14) and are shown graphically in Fig. 12(a) for various values of viscosity and thermal conductivity parameters for air and water. It increases with time and reaches the steady state after a certain time lapse. It is observed that average skin friction decreases with the increasing value of viscous parameter λ, pressure work parameter Ge and heat generation parameter Q. It is also observed that average wall shear stress increases with the increasing value of thermal conductivity parameter γ. An increase in the value of Prandtl's number, average skin friction are found to decrease.

Figures 11(b) shows dimensionless steady state local heat transfer rate for air and water for different values of variation parameters. It is found that local heat transfer rate increases as viscosity parameter, thermal conductivity parameter and heat generation parameter increases. The local heat transfer rate increases with increasing value of *Pr.* This trend is expected because larger *Pr* results in a thinner thermal boundary layer, with a corresponding larger wall temperature gradient and hence a larger heat transfer rate. In Fig. 12(b), the effects of variation parameters and *Pr* on average Nusselt number are shown. An increase in the Prandtl's number lead to an increase in the average heat transfer rate, because increasing the Prandtl's number speeds up the spatial decay of the temperature in the flow field, yielding an increase in the rate of heat transfer and also same manner for heat generation parameter. It is also observed that average Nusselt's number decreases as λ , γ and *Q* increases.

Table-1: Velocity values of Variation of dimensionless velocity profiles against dimensionless y for different values of variable thermal conductivity parameter Y with Pr = 0.733, λ= 0.40, Ge=0.00 and Q = 0.00.

Y	Y=0			Y=2			Y=4		
	Present	G.palani Kwang-Yong Kim	Elbashbeshy & Ibrahim	Present	G.palani Kwang-Yong Kim	Elbashbeshy & Ibrahim	Present	G.palani Kwang-Yong Kim	Elbashbeshy & Ibrahim
	U(X,Y)	U(X,Y)	U(X,Y)	U(X,Y)	U(X,Y)	U(X,Y)	U(X,Y)	U(X,Y)	U(X,Y)
0.000	0.000	0.000	0.000	0.000	0.000	0.000	0.000	0.000	0.000
1.000	0.444	0.446	0.443	0.547	0.556	0.552	0.575	0.585	0.581
2.000	0.465	0.468	0.465	0.589	0.598	0.594	0.673	0.684	0.680
3.000	0.314	0.316	0.314	0.377	0.387	0.383	0.488	0.499	0.495
4.000	0.143	0.147	0.144	0.211	0.219	0.216	0.279	0.288	0.284
5.000	0.076	0.079	0.077	0.087	0.097	0.095	0.135	0.142	0.139
6.000	0.034	0.036	0.033	0.026	0.038	0.034	0.040	0.049	0.045
7.000	0.009	0.014	0.011	0.006	0.009	0.008	0.009	0.018	0.014
8.000	0.000	0.000	0.021	0.000	0.000	0.000	0.000	0.000	0.000

Fig. 2(a) Velocity profiles shown for various values of dependent thermal conductivity comparing our present work with the work of G.palani Kwang-YongKim and Elbashbeshy & Ibrahim. The data from the figures are in good agreement with our present work.

4. CONCLUSION

The influence of changing viscosity and thermal conductivity on heat generation laminar natural convection boundary-layer vertical plate with pressure work is analyzed in this work. The thermal conductivity is assumed to be a linear function of temperature and the fluid viscosity is expected to fluctuate as an exponential function. An implicit Crank-Nicolson type finite difference approach is used to solve the dimensionless governing equations. Graphically, a comparison is drawn between the current numerical findings and previously published research. The agreement between the two parties is seen to be great. The present analysis has shown that:

(i) The dimensionless fluid velocity rises as the viscosity parameter λ increases and the fluid temperature falls. Greater velocity is found in a location near the wall when the viscosity variation parameter λ is large, resulting in a higher Nusselt number and reduced skin friction.

(ii) The fluid velocity, fluid temperature, the dimensionless wall velocity gradient, and the dimensionless rate of heat transfer from the plate to the fluid all rise as the thermal conductivity parameter γ increases.

(iii) It has been discovered that ignoring the viscosity and thermal conductivity variations would result in significant inaccuracies. As a consequence, we suggest that the impacts of changing viscosity and thermal conductivity must be addressed in order to anticipate more accurate outcomes.

(iv) When the work parameter Ge is increased for the impact of pressure, the velocity profiles are somewhat increased. Furthermore, when the pressure work parameter rises, the temperature profile rises.

(v) When the Heat generation parameter Q is increased, the velocity and temperature profiles are significantly increased.

(vi) The variation of heat generation parameter *Q*, Pressure work parameter, variable viscosity parameter and temperature dependent parameter, the local skin friction coefficient, the local Nusselt number and the velocity distribution over the whole boundary layer decreases, but the temperature distribution increases.

REFERENCES

[1] Sree Pradip Kumer Sarker, Md. M. Alam Effects of variable viscosity and thermal conductivity on MHD natural convection flow a vertical flat plate, Journal of Advances in Mathematics and Computer Science, 2021; 36(3): 58-71.

[2] Alam MM, Alim MA, Chowdhury MMK. Effect of pressure stress work and viscous dissipation in natural convection flow along a vertical flat plate with heat conduction, Journal of Naval Architecture and Marine Engineering, 2006;3(2): 69-76.

[3] Alim M A, Alam MM, Al-Mamun Abdullah, Joule heating effect on the coupling of conduction with magneto-hydrodynamic free convection flow from a vertical flat plate, Nonlinear Analysis: Modeling and Control. 2007;.12(3): 307-316.

[4] Rahman M.M, Mamun A A, Azim MA, Alim MA, Effects of temperature dependent thermal conductivity on MHD free convection flow along a vertical flat plate with heat conduction, Nonlinear Analysis: Modeling and Control. 2008;13(4): 513-524.

[5] Alim MA, Alam MM, Al-Mamun Abdullah Hossain Belal, The combined effect of viscous dissipation & Joule heating on the coupling of conduction & free convection along a vertical flat plate. International Communications in Heat and Mass Transfer. 2008; 35(3): 338-346.

[6] Safiqul Islam A.KM, Alim M A, Sarker MMA, Khodadad Khan AFM, Effects of temperature dependent thermal conductivity on natural convection flow along a vertical flat plate with heat generation, Journal of Naval Architecture and Marine Engineering. 2012;9(2): 113-122.

[7] Kabir KH, Alim MA, Andallah LS, Effects of viscous dissipation on MHD natural convection flow along a vertical wavy surface. Journal of Theoretical and Applied Physics. an Springer Open Journal. 2013; 7(31) 1-8.

[8] Hossain MA, Viscous and Joule heating effects on MHD free convection flow with variable plate temperature. 1992; 35 (2): .3485-3487.

[9] Soundalgekar, VM, Ganesan, P, Finite difference analysis of transient free convection on an isothermal flat plate. Reg. J. Energy Heat Mass Transf. 1981; 3; 219-224.

[10] Elbashbeshy, EMA, Ibrahim, FN, Steady free convection flow with variable viscosity and thermal diffusivity along a vertical plate. J. Phys. D Appl. Phys. 1993;26(12): 237-2143.

[11] Kafoussius, NG, Rees, DAS, Numerical study of the combined free and forced convective laminar boundary layer flow past a vertical isothermal flat plate with temperature dependent viscosity. Acta Mech. 1998; 127(11): 39-50.

[12] Elbashbeshy, EMA, Dimian, MF, Effect of radiation on the flow and heat transfer over a wedge with variable viscosity. Appl. Math. Comput. 2002; 132: 445-454.

[13] Anwar Hossain, Khalil M, K., Kambi MV, The effect of radiation on free convection flow of fluid with variable viscosity from a porous vertical plate. Int. J. Therm. Sci. 2001;40: 115-124.

[14] Seddeek, MA, Effect of variable viscosity on a MHD free convection flow past a semi-infinite flat plate with an aligned magnetic field in the case of unsteady flow. Int. J. Heat Mass Transf. 2002; 45: 931-935.

[15] Carnahan B, Luther HA, Wilkes JO, Applied Numerical Methods. Wiley, New York.1969.

[16] Siattery, J.C Momentum, Energy and Mass Transfer in Continua. McGraw Hill, New York. 1972.

[17] Ockendon, H, Ockendon, JR, Variable-viscosity flows in heated and cooled channels. J. Fluid Mech. 1977; 83(1): 177-190.

[18] Seddeek, MA., Abdelmeguid, MS, Effects of radiation and thermal diffusivity on heat transfer over a stretching surface with variable heat flux. Phys. Lett. A . 2006; 348(3-6): 172-179.

[19] Palani, G, and Kim, KY, Numerical study on vertical plate with variable viscosity and thermal conductivity. Springer-Verlag. 2009; 80: 711-725.

[20] Carnahan, B, Luther, HA, Wilkes, JO, Applied Numerical Methods. Wiley, New York. 1969.

[21] Ullah A, Shah Z, Kumam P, Ayaz M, Islam S, Jameel M. Viscoelastic MHD Nanofluid Thin Film Flow over an Unsteady Vertical Stretching Sheet with Entropy Generation. *Processes*. 2019; 7(5):262. https://doi.org/10.3390/pr7050262

[22] Ullah A, Hafeez A, Mashwani WK, Ikramullah, Kumam W, Kumam P, Ayaz M. Non-Linear Thermal Radiations and Mass Transfer Analysis on the Processes of Magnetite Carreau Fluid Flowing Past a Permeable Stretching/Shrinking Surface under Cross Diffusion and Hall Effect. *Coatings*. 2020; 10(6):523. https://doi.org/10.3390/coatings10060523

[23] Abdeljawad T, Ullah A, Alrabaiah H, Ikramullah, Ayaz M, Khan W, Khan I, Khan HU. Thermal Radiations and Mass Transfer Analysis of the Three-Dimensional Magnetite Carreau Fluid Flow Past a Horizontal Surface of Paraboloid of Revolution. *Processes*. 2020; 8(6):656. https://doi.org/10.3390/pr8060656